

## A Planet Candidate Orbiting near the Hot Jupiter TOI-2818 b Inferred through Transit Timing

BRENDAN J. MCKEE <sup>1</sup> BENJAMIN T. MONTET <sup>1,2</sup> SAMUEL W. YEE <sup>3,4,\*</sup> JOEL D. HARTMAN <sup>3</sup>  
JOSHUA N. WINN <sup>3</sup> JORGE H. C. MARTINS <sup>5</sup> ANDRÉ M. SILVA <sup>6</sup> AND ALEXANDER L. WALLACE <sup>7</sup>

<sup>1</sup>*School of Physics, University of New South Wales, Sydney, NSW 2052, Australia*

<sup>2</sup>*UNSW Data Science Hub, University of New South Wales, Sydney, NSW 2052, Australia*

<sup>3</sup>*Department of Astrophysical Sciences, Princeton University, 4 Ivy Lane, Princeton, NJ 08544, USA*

<sup>4</sup>*Center for Astrophysics | Harvard & Smithsonian, 60 Garden St, Cambridge, MA 02138, USA*

<sup>5</sup>*Instituto de Astrofísica e Ciências do Espaço, Universidade do Porto, Rua das Estrelas, 4150-762 Porto, Portugal*

<sup>6</sup>*Instituto de Astrofísica e Ciências do Espaço, Universidade de Lisboa, Campo Grande, 1749-016 Lisboa, Portugal*

<sup>7</sup>*School of Physics and Astronomy, Monash University, Victoria 3800, Australia*

### ABSTRACT

TOI-2818 b is a hot Jupiter orbiting a slightly evolved G-type star on a 4.04-day orbit that shows transit timing variations (TTVs) suggestive of a decreasing orbital period. In the most recent year of TESS observations, transits were observed  $\sim 8$  minutes earlier than expected for a constant period. The implied orbital decay rate is  $1.35 \pm 0.25$  s yr<sup>-1</sup>, too fast to be explained by tidal dissipation even considering the evolved nature of the host star. Radial velocity monitoring and astrometric data make the possibility of perturbations from a long-period companion unlikely; further Doppler spectroscopy observations can efficiently confirm or rule out such a companion. Apsidal precession due to the tidal distortion of the planet is also physically implausible. The most plausible explanation for the TTVs appears to be gravitational perturbations from a hitherto undetected planet with mass  $\lesssim 10 M_{\oplus}$  that is in (or near) a mean-motion resonance with the hot Jupiter. Such a planet could be responsible for the observed TTVs while avoiding detection with the available radial velocity and transit data.

*Keywords:* Exoplanet tides (497) — Exoplanets (498) — Hot Jupiters (753) — Radial velocity (1332)  
— Transit photometry (1709) — Transit timing variation method (1710)

### 1. INTRODUCTION

Hot Jupiters can exhibit transit timing variations (TTVs) arising from tidal interactions, apsidal precession, or companion planets or stars. Tidal interactions allow the star and planet to exchange rotational and orbital angular momentum, which for many hot Jupiters is expected to lead to orbital decay (Patra et al. 2020). Searches for orbital decay in hot Jupiters have yielded a high-confidence detection of tidal decay, WASP-12 b (Yee et al. 2020) and a second candidate, Kepler-1658 b (Vissapragada et al. 2022). WASP-12 b is a hot Jupiter on a 1-day orbit decaying by  $\sim 30$  ms yr<sup>-1</sup>, while Kepler-1658 b is on a 4-day orbit decaying by  $\sim 130$  ms yr<sup>-1</sup>. When interpreted within a simple theory in which the

equilibrium tidal bulge is displaced by a constant lag angle, the implied modified tidal quality factors, the ratio between energy stored in tidal distortions and energy dissipated by friction, are  $Q'_* \sim 10^5$  for WASP-12 b and  $Q'_* \sim 10^4$  for Kepler-1658 b. Such low  $Q'_*$  values are only expected if the star is a subgiant or there are nonlinear effects such as wave breaking (Weinberg et al. 2017; Barker 2020). Tidal inspiral is expected to occur in many systems, although the size of the effect makes unambiguous confirmation difficult (Patra et al. 2020).

Apsidal precession can also produce quasi-sinusoidal TTVs (Patra et al. 2017; Yee et al. 2020). The time interval between transits will oscillate slightly as the line of apsides of the elliptical orbit rotates relative to the line of sight. Steady acceleration of the star toward or away from us, due to a massive long-period companion can also create the illusion of a changing period due to the Rømer effect, also called light travel time delay, as has been proposed for the WASP-4 system

Corresponding author: Brendan J. McKee  
b.mckee@unsw.edu.au

\* 51 Pegasi b Fellow

(Bouma et al. 2020), and observed in triple star systems through eclipse timing variations (Borkovits et al. 2016). In many exoplanet systems TTVs are caused by gravitational interactions with nearby or massive planets. Most hot Jupiter systems do not have detectable nearby companions (Hord et al. 2021), although there are a few counterexamples, such as WASP-47 (Becker et al. 2015), WASP-84 (Maciejewski et al. 2023), WASP-132 (Hord et al. 2022), Kepler-730 (Cañas et al. 2019), and TOI-2000 (Sha et al. 2023). For WASP-47 (Becker et al. 2015) and TOI-1130 (Huang et al. 2020; Korth et al. 2023), detectable TTVs have been induced by the nearby companions in these systems. Analysis of hot Jupiter TTVs in the *Kepler* data set suggests that  $\sim 12\%$  of hot Jupiter systems may have unseen nearby companions (Wu et al. 2023).

TTVs can have small amplitudes and long periods, necessitating long observing baselines to detect them. The *TESS* mission (Ricker et al. 2015) has entered its fifth year of operation and is now revisiting southern hemisphere targets four years after first observing them. For stars outside of the continuous viewing zone, this typically means the available data consist of 1–2 months of coverage with two-year gaps between them. Any slow changes in transit timing might be invisible across a few months, but detectable over several years.

Such is the case for the hot Jupiter orbiting the slightly evolved G-type star TOI-2818. Yee et al. (2023) discovered TOI-2818 b, a hot Jupiter on a 4-day orbit, using *TESS* data from Sectors 7, 8, and 34, and confirmed using ground-based transit and radial velocity data. *TESS* has now re-observed the system in Sector 61, and as shown in this work, the transits were observed several minutes earlier than expected if the period were constant.

In this paper we use these data, along with ground-based light curves and precise radial-velocity data, to explore the possibilities of orbital decay, apsidal precession, the Rømer effect, and close companion planets as mechanisms to explain the observed timing variations. The rest of this paper is organized as follows. In Section 2 we analyze and process the transit light curves and radial velocity measurements. In Section 3 we fit the transit timing variations and radial velocity data to different models. In Section 4 we present our conclusions.

## 2. DATA

### 2.1. *TESS* Photometry

*TESS* observed TOI-2818 in Sectors 7, 8, 34 and 61, providing a baseline that extends from 2019 January 7 to 12 February 2023. We used the shortest cadence data available for each sector. In years 1 and 3 of the mis-

sion, the target only appears in the *TESS* full-frame images (FFIs). We used light curves at 1800-second cadence for Sectors 7 and 8 and 600-second cadence for Sector 34 from the *TESS* Quick Look Pipeline (QLP) (Huang et al. 2020a,b; Kunimoto et al. 2021). In year 5 *TESS* observed TOI-2818 at 120-second cadence; for Sector 61 we used the pre-search data conditioning simple aperture photometry light curves produced by the Science Processing Operations Center pipeline (Smith et al. 2012; Stumpe et al. 2014; Jenkins et al. 2016). We downloaded both datasets from the Milkuski Archive for Space Telescopes (STSci 2021, 2022). We selected a one-day long section around each transit to separate the transits and fit them individually.

### 2.2. Ground-based Photometry

Yee et al. (2023) described observations of two transits of TOI-2818 b by ground-based telescopes on 2021 December 8 and 2021 December 12 using the 0.51 m telescope at the El Sauce Observatory and a 0.4 m telescope as part of the Las Cumbres Observatory at the Cerro Tololo Inter-American Observatory (CTIO) respectively. These data are publicly available through ExoFOP (NExSci 2022)<sup>1</sup>.

### 2.3. Radial Velocity Observations

Yee et al. (2023) report 7 radial velocity measurements of TOI-2818 recorded between 2021 December 21 and 2022 March 15 by the CTIO High Resolution Spectrometer (CHIRON; Tokovinin et al. (2013); Paredes et al. (2021)) on the CTIO 1.5 m telescope. We removed one observation from our analysis as it was collected during the transit of TOI-2818 b, to avoid the impact of the Rossiter-McLaughlin effect on the measured radial velocity. We collected two new measurements on 2023 June 2 and 2023 June 4 following the same methodology.

We obtained eight radial velocity measurements taken with VLT/ESPRESSO (Echelle SPectrograph for Rocky Exoplanets and Stable Spectrographic Observations; Pepe et al. (2021)). Seven observations were taken between 2023 June 19 and 2023 June 28, and an eighth on 2023 September 5, under program ID 111.264Q (PI Montet). All exposures were 600 seconds in length, using a sky fiber for background subtraction and read out in the slow readout mode with 2x1 binning. We infer the stellar RV and its uncertainty at each observation time through the ESPRESSO DRS pipeline v3.2.0. These radial velocity measurements are recorded in Table 1.

<sup>1</sup> <https://exofop.ipac.caltech.edu/tess>

**Table 1.** Radial Velocity Measurements of TOI-2818

Source	Time (BJD <sub>TDB</sub> )	RV (m s <sup>-1</sup> )	Uncertainty (m s <sup>-1</sup> )
CHIRON <sup>1</sup>	2459569.7244	58907	30
CHIRON <sup>1</sup>	2459571.7617	59038	30
CHIRON <sup>1</sup>	2459595.7596	59071	23
CHIRON <sup>1</sup>	2459597.7544	58868	27
CHIRON <sup>1</sup>	2459620.5707	59093	33
CHIRON <sup>1</sup>	2459622.5622	58920	27
CHIRON <sup>1,2</sup>	2459653.5862	59081	24
CHIRON	2460097.5217	59082	26
CHIRON	2460099.5086	59023	51
VLT/ESPRESSO	2460115.4623	60380.8	1.8
VLT/ESPRESSO	2460116.4475	60473.9	2.6
VLT/ESPRESSO	2460117.4540	60519.4	2.8
VLT/ESPRESSO	2460118.4547	60407.9	8.3
VLT/ESPRESSO	2460122.4548	60417.9	6.2
VLT/ESPRESSO	2460123.4499	60368.8	2.3
VLT/ESPRESSO	2460124.4581	60463.6	2.1
VLT/ESPRESSO	2460192.8707	60438.7	5.2
$\gamma_{\text{CHIRON}}$		58993	11
$\gamma_{\text{VLT/ESPRESSO}}$		60445.0	1.5

NOTE—<sup>1</sup> Data from [Yee et al. \(2023\)](#). <sup>2</sup> Value measured during transit, removed from analysis due to Rossiter-McLaughlin effect.

**Table 2.** Transit Times for TOI-2818 b

Source	Transit Time (BJD <sub>TDB</sub> )	Uncertainty (days)	Epoch
<i>TESS</i> Sector 7	2458494.2454	0.0011	0
<i>TESS</i> Sector 7	2458498.2820	0.0011	1
<i>TESS</i> Sector 7	2458502.3240	0.0011	2
<i>TESS</i> Sector 7	2458506.3639	0.0011	3
<i>TESS</i> Sector 7	2458510.4043	0.0012	4
<i>TESS</i> Sector 7	2458514.4414	0.0010	5
<i>TESS</i> Sector 8	2458518.4830	0.0011	6
<i>TESS</i> Sector 8	2458522.5208	0.0012	7
<i>TESS</i> Sector 8	2458530.6008	0.0012	9
<i>TESS</i> Sector 8	2458538.6828	0.0012	11
<i>TESS</i> Sector 34	2459229.4745	0.0009	182
<i>TESS</i> Sector 34	2459233.5141	0.0010	183
<i>TESS</i> Sector 34	2459237.5519	0.0009	184
<i>TESS</i> Sector 34	2459245.6328	0.0010	186
<i>TESS</i> Sector 34	2459249.6702	0.0009	187
<i>TESS</i> Sector 34	2459253.7110	0.0009	188
El Sauce	2459556.6885	0.0006	263
LCO CTIO	2459560.7284	0.0021	264
<i>TESS</i> Sector 61	2459964.6962	0.0008	364
<i>TESS</i> Sector 61	2459968.7376	0.0007	365
<i>TESS</i> Sector 61	2459972.7753	0.0008	366
<i>TESS</i> Sector 61	2459980.8553	0.0008	368
<i>TESS</i> Sector 61	2459984.8947	0.0008	369

#### 2.4. Model Fitting

We fit the light curves following a similar methodology to that described in [McKee & Montet \(2023\)](#) using the python `exoplanet` package ([Foreman-Mackey et al. 2021a](#)). We fit each *TESS* transit using common limb darkening coefficients  $u_1$  and  $u_2$  following the reparameterization of [Kipping \(2013\)](#), while each ground-based transit used different limb darkening coefficients.

We sampled the planet radius  $R_b$  and impact parameter  $b$  from log uniform and uniform priors respectively; these parameters are shared for each transit. We assigned priors for the mass  $M_\star$  and radius  $R_\star$  of the star as inferred from the spectral analysis of [Yee et al. \(2023\)](#). The mean out-of-transit flux value was allowed to vary for each transit. We included a quadratic model for the out of transit flux in the ground-based photometry to account for atmospheric effects. Given the proximity of the planet to the star, and the theoretical presumption that the eccentricity has been damped to an undetectably low level, we fix the eccentricity of the orbit to 0 for the light curve fitting. We allowed the mid-transit time of

each transit to be a free parameter, in order to search for TTVs. We sampled each posterior distribution with `PyMC3` ([Salvatier et al. 2016](#)), with 8,000 tuning steps and 40,000 draws. We verified our chains converged via visual inspection and following the diagnostic of [Geweke \(1992\)](#). The mid-transit times found are listed in [Table 2](#). The light curve fit to each year of transits is presented in [Figure 2](#).

We jointly fit a circular orbit to the TTVs and the RVs using the python `TTVFast` package ([Deck et al. 2014](#)). We use `TTVFast` here to remain consistent with later models which model interactions between multiple planets. We assign a mass  $M$ , period  $P$ , longitude of the ascending node  $\Omega$ , and mean longitude  $\lambda$  to the planet. We fix the longitude of the ascending node for the planet as  $\Omega_b = 0$ , as it can not be inferred from the available data. We fix the inclination to  $i = 88.3^\circ$ , calculated from the best fit light curve model. The stellar mass is fit with the same prior as previously, for all other parameters we apply a uniform prior. We fit independent offsets for

the two sources of radial velocities. We also included jitter terms added in quadrature to the uncertainties from *TESS* years 1, 3 and 5 separately, each ground-based transit, and CHIRON and ESPRESSO RVs. The model is started at a time of BJD 2458494. This model is the basis of the linear ephemeris used in Figure 1. The fit of the radial velocities is shown in Figure 2.

We also fit a model with a linear acceleration term to the radial velocity to identify long-term trends, finding  $\dot{v}_r = +0.08 \pm 0.05 \text{ m s}^{-1} \text{ day}^{-1}$ . Table 3 gives the mass and period of the planet found with and without an acceleration term.

### 3. ANALYSIS

#### 3.1. *Tidal Inspiral*

A decaying orbit with a period that decreases at a constant rate will produce quadratic TTVs. We generated transit times and RVs for a circular orbit with a constant period with *TTVFast*, then applied a correction to the transit times to simulate a decaying period. The correction factor added is

$$\Delta t = \frac{1}{2} \frac{dP}{dN} N^2, \quad (1)$$

where  $P$  is the period of the planet and  $N$  the transit epoch, following Patra et al. (2017). We sampled with *emcee* (Foreman-Mackey et al. 2013), an implementation of the affine invariant MCMC sampler of Goodman & Weare (2010), with the maximum-likelihood fit used as starting conditions for an N-body integration. We sample with 100 walkers and 10,000 steps, with the first 9,000 discarded as burn-in. The results of this fitting are listed in Table 3.

The TTVs produced are displayed in Figure 1. We find a best-fitting decay rate of  $1.35_{-0.26}^{+0.24} \text{ s yr}^{-1}$ . This is more than an order of magnitude larger than the decay rate for both WASP-12 b ( $29 \pm 2 \text{ ms yr}^{-1}$ , Yee et al. 2020) and Kepler-1658 b ( $131_{-22}^{+20} \text{ ms yr}^{-1}$ , Vissapragada et al. 2022). The decay timescale of this system under this model,  $P/\dot{P}$ , is  $270_{-50}^{+70} \text{ kyr}$ , a factor of 10 shorter than the other planets.

If the cause of this decay is tidal dissipation then within the framework of the simplified tidal model of Goldreich & Soter (1966) we can determine the modified tidal quality factor,  $Q'_*$ , of the planet as

$$\dot{P} = -\frac{27\pi}{2Q'_*} \left( \frac{M_p}{M_*} \right) \left( \frac{R_*}{a} \right)^5, \quad (2)$$

where  $a$  is the semi-major axis of the planet's orbit. For this system we calculate a tidal quality factor of

$$Q'_* = 10.1_{-1.5}^{+2.2}. \quad (3)$$

**Table 3.** Parameters at BJD 2458494

Parameter	Value	Uncertainty
<b>Constant Period Model</b>		
Period (days)	4.039705	$+0.000006$ $-0.000002$
Planet Mass ( $M_{\text{Jup}}$ )	0.61	$\pm 0.03$
<b>Linear Acceleration Model</b>		
Period (days)	4.039706	$+0.000007$ $-0.000002$
Planet Mass ( $M_{\text{Jup}}$ )	0.60	$\pm 0.03$
Acceleration ( $\text{m s}^{-1} \text{ day}^{-1}$ )	0.08	$\pm 0.05$
<b>Decaying Period Model</b>		
Period (days)	4.039736	$\pm 0.000006$
Planet Mass ( $M_{\text{Jup}}$ )	0.60	$\pm 0.03$
Decay Rate ( $\text{days orbit}^{-1} \times 10^{-7}$ )	-1.7	$\pm 0.3$
Tidal Quality Factor $Q'_*$	10.1	$+2.2$ $-1.5$
Rømer Acceleration ( $\text{m s}^{-1} \text{ day}^{-1}$ )	-3.2	$\pm 0.5$
<b>Outer Companion Model</b>		
Period (days)	4.039697	$+0.000006$ $-0.000004$
Planet Mass ( $M_{\text{Jup}}$ )	0.61	$+0.06$ $-0.03$
Eccentricity	0.014	$+0.005$ $-0.007$
Argument of Periastron (deg)	-24	$\pm 25$
Companion Period (days)	2150	$+330$ $-350$
Companion Mass ( $M_{\text{Jup}}$ )	71	$+35$ $-30$
Companion Eccentricity	0.84	$+0.07$ $-0.12$
Companion Argument (deg)	9	$+9$ $-8$
<b>Apsidal Precession Model</b>		
Period (days)	4.039709	$+0.000022$ $-0.000010$
Planet Mass ( $M_{\text{Jup}}$ )	0.61	$\pm 0.03$
Eccentricity	0.004	$+0.004$ $-0.003$
Argument of Periastron (deg)	-50	$+40$ $-70$
<b>Best 16-Day Planet Model</b>		
Period (days)	4.03972459	
Planet Mass ( $M_{\text{Jup}}$ )	0.493477	
Eccentricity	0.0115	
Argument of Periastron (deg)	-38.18	
Companion Period (days)	16.1953744	
Companion Mass ( $M_{\oplus}$ )	13.976203	
Companion Eccentricity	0.0671	
Companion Argument (deg)	47.87	

This result is orders of magnitude smaller than the values reported for WASP-12 b and Kepler-1658 b of  $1.75_{-0.11}^{+0.13} \times 10^5$  and  $2.50_{-0.62}^{+0.85} \times 10^4$  respectively. The tidal quality is typically at least  $10^5 - 10^7$  for hot Jupiters, but can be lower if the star is a subgiant such as WASP-12 (Weinberg et al. 2017). TOI-2818 is closer to the main sequence than WASP-12. Nonlinear effects such as wave

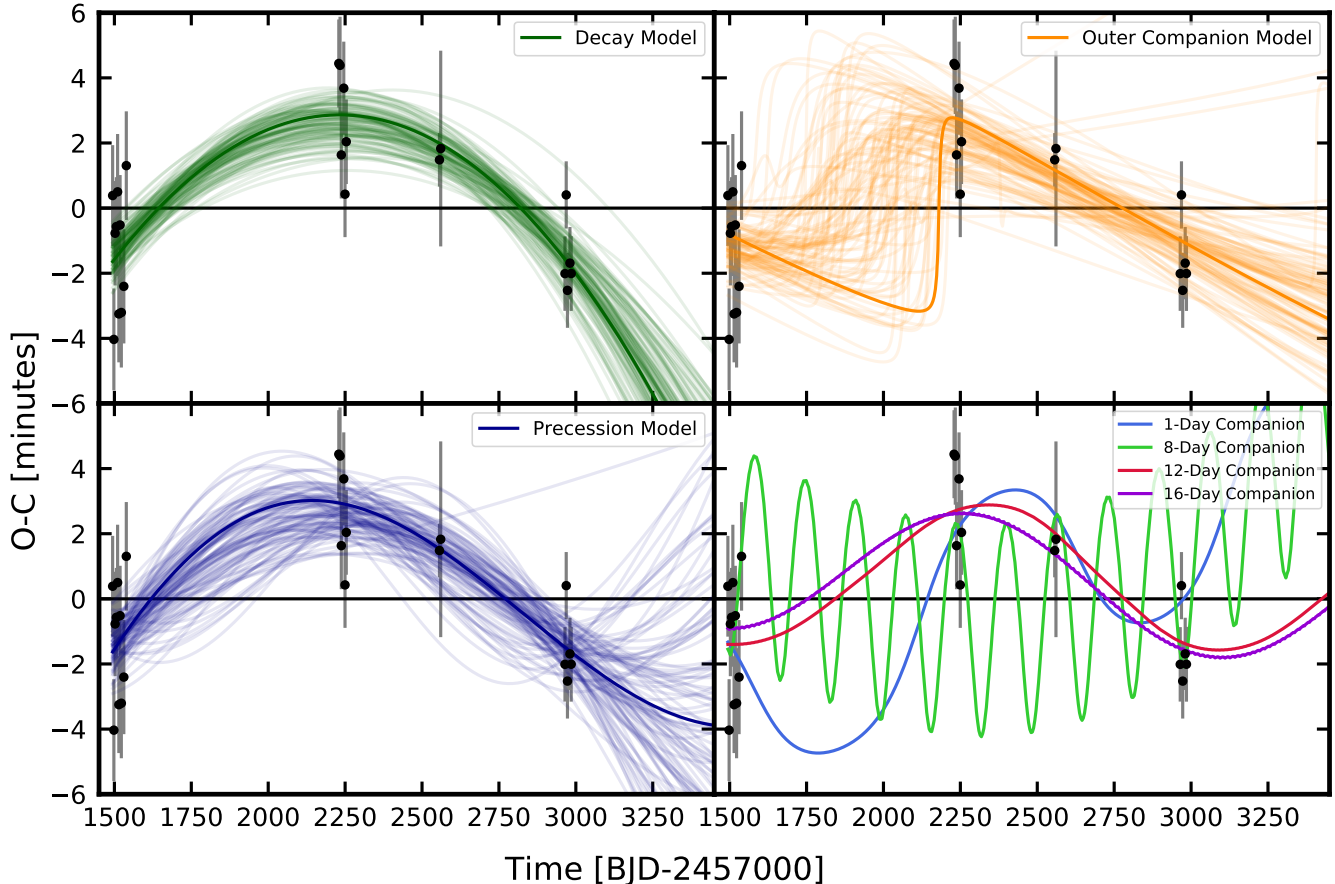


**Figure 1.** TTV models are compared to the measured mid-transit times that are displayed as black points. The black line represents a linear ephemeris. The top left panel shows representative samples of the decay model in transparent green, along with the best fit as a solid line. The top right and bottom left panels show the same for the outer companion acceleration model (orange) and apsidal precession model (blue) respectively. The bottom right panel show the best fitting models featuring companion planets at 1 (blue), 8 (green), 12 (red) and 16 days (purple). Each type of model can fit the TTVs, but other constraints make all but the planetary model physically implausible.

breaking can also result in smaller tidal quality factors, although not as low as 10 (Barker 2020).

### 3.2. Rømer Delay

The same quadratic TTV effect can be observed if the star is being accelerated steadily along the line of sight towards the observer due to the Rømer effect. A constant acceleration causes an apparent change in period given by

$$\frac{\dot{P}}{P} \approx \frac{\dot{v}_r}{c}, \quad (4)$$

where  $\dot{v}_r$  is the change in line of sight velocity. The implied acceleration of TOI-2818 is  $-3.2^{+0.5}_{-0.5} \text{ m s}^{-1} \text{ day}^{-1}$ . This is significantly larger than the  $\dot{v}_r = +0.08^{+0.05}_{-0.05} \text{ m s}^{-1} \text{ day}^{-1}$  inferred from Doppler spectroscopy as calculated in Section 2.

### 3.3. Acceleration by an Outer Companion

A constant acceleration throughout the timespan of the data has been ruled out by the lack of an RV trend. Very wide binaries beyond  $\sim 300 \text{ AU}$  are excluded by high-resolution imaging (Yee et al. 2023). A nearer (few AU) companion to the system would produce an acceleration that is not necessarily constant over the timespan of the data; instead inducing Keplerian motion of the star/planet system. The acceleration will cause the observed transits to appear closer together or further apart as the light travel time changes at a non-constant rate. This more complex model might be compatible with the TTVs and radial velocity measurements, given the uneven time sampling of both types of data.

To test this we include a  $\sim 50M_{\text{Jup}}$  brown dwarf in our TTVFast model, allowing the same parameters as for the planet to vary, with the addition of initial eccentricity  $e$ , and argument of periapsis  $\omega$ . In order to determine the

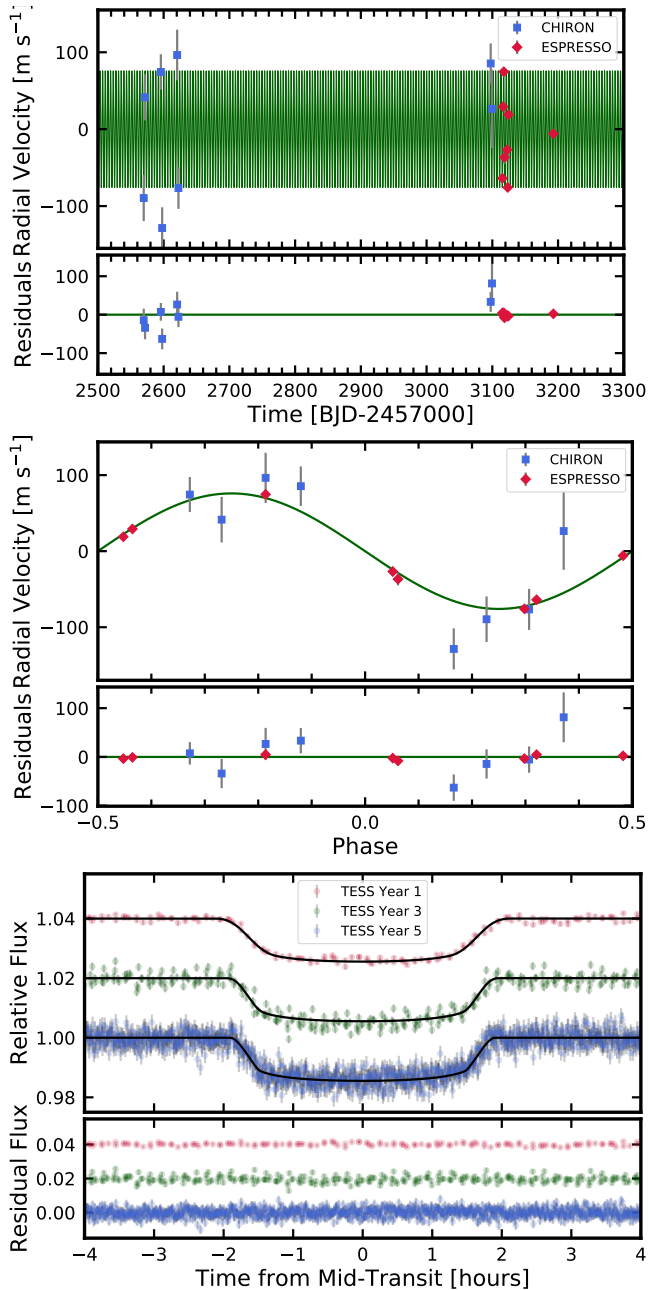


**Figure 2.** The top panels show the radial velocities measured by CHIRON (blue) and VLT/ESPRESSO (red) compared to the best-fitting circular orbit model over the observation baseline, the panel below shows the residuals. The middle panel shows the radial velocities folded over the phase of the orbit, with the residuals below. A circular orbit is a good fit to the data. The bottom panels show the light curves of the transits aligned to the mid-transit times. Each year is stacked together, with vertical offsets between years 1 (red), 3 (green) and 5 (blue). The panel below shows the residuals to the light curve fit in the same fashion. The depth and duration of the transit does not change between each year of observations.

TTVs, we calculate the light travel time delay between the star and the center of mass of the system. `TTVFast` does not account for this effect, and does not provide the three-dimensional coordinates of the star at the time of each transit. Instead we integrate the radial velocity of the star to infer the radial position of the star. We convert this distance into light travel time and correct the transit times. We again sample with `emcee` (Foreman-Mackey et al. 2013), in the same manner as previously. The results of this fitting are listed in Table 3. Samples of the model are shown in Figure 1.

We find that the results favor a companion of  $\sim 70M_{\text{Jup}}$  and a  $\sim 2,100$ -day period. The orbit has  $e \approx 0.8$ , and an argument of periapsis nearly perpendicular to the line of sight at an angle of  $9 \pm 9^\circ$ . This allows the radial velocities to have little variation across the observation interval, consistent with the lack of RV trend over our observing baseline. The companion induces an acceleration of  $\sim 60 \text{ m s}^{-1} \text{ yr}^{-1}$ , with a short RV shift up to  $\sim 2500 \text{ m s}^{-1}$  at periastron. Additional radial velocity observations with CHIRON or ESPRESSO in particular could quickly detect or rule out such a companion.

This orbital configuration avoids RV detection by shifting motion from the line of sight to the plane of the sky. This should produce an astrometric signal that could be measured by *Gaia* (Gaia Collaboration et al. 2016). The renormalized unit weight error (RUWE) is a measure of how well a single-star model fits to the data measured by *Gaia* (Lindgren et al. 2018, 2021). This measure is sensitive to unresolved stellar companions (Belokurov et al. 2020). The RUWE is expected to be around 1.0 for a good fit, a higher value may indicate that the source is not a single star. The RUWE from *Gaia* DR3 for this system is 0.924 (Gaia Collaboration et al. 2023) We simulated the expected RUWE for this system using the procedure described in Wallace et al. (2024). Simulating a brown dwarf in the requisite orbit produces a RUWE 0.924 or smaller only 7% of the time, compared to 22% of the time for single star models. The outer companion solution is therefore less likely to explain the RUWE than solutions that do not include a brown dwarf. The predicted RUWE is dependent on the time of periapse of the companion: due to the high eccentricity, there is relatively little orbital motion for much of the orbital period. By chance, *Gaia* DR3 observations do not contain the expected time of periapse; if the brown dwarf exists we expect the RUWE over a full orbit to be as high as 1.7. *Gaia* DR4 should provide the astrometric data over a long enough baseline to detect or rule out this hypothetical companion.

Despite fitting the transits well, the high eccentricity and short orbit result in a close periastron of  $< 0.7$  AU. A large companion this close to the host star will truncate the protoplanetary disk, presenting challenges for Jupiter-sized planet formation (Jang-Condell 2015). It is possible that the current orbital configuration was not present at formation and that the eccentricity of the brown dwarf was excited over time, possibly through dynamical interactions with another companion. The close passes of the companion can introduce dynamic instability to the system, which may not survive. The best-fitting solution is stable over a timescale of 100,000 years, however the Lyapunov time is only 200 years, suggesting that the system is chaotic.

In summary, an outer companion can explain the observations, but requires specific orbital configurations and coincidences in observation timing to evade detection. Additional RV or astrometric data should be conclusive about the possibility of a brown dwarf in this system as the cause of the TTVs.

### 3.4. Apical Precession

Apsidal precession can create sinusoidal TTVs due to the change of orientation of the elliptical orbit of the planet in time. We use the same method as previously described by using `TTVFast` to create an eccentric orbit with constant period, then applying a correction factor to the transit times. The correction applied is:

$$\Delta t = -\frac{eP_a}{\pi} \cos \omega(N), \quad (5)$$

$$\omega(N) = \omega_0 + \frac{d\omega}{dN}N, \quad (6)$$

$$P_s = P_a \left( 1 - \frac{1}{2\pi} \frac{d\omega}{dN} \right), \quad (7)$$

as described by Giménez & Bastero (1995), and adapted to the low eccentricity, high inclination limit by Patra et al. (2017). We again sample with `emcee` (Foreman-Mackey et al. 2013), in the same manner as previously. The results of this fitting are listed in Table 3. We find that the best-fitting eccentricity is  $0.004^{+0.004}_{-0.003}$  with a best-fitting precession rate of  $38^{+25}_{-14}$  yr $^{-1}$ . The model is shown in Figure 1.

This precession rate is high and difficult to explain from a theoretical perspective. The theoretical precession rate in most hot Jupiter systems is thought to be dominated by the contribution from the planetary tidal bulge, which can be used to calculate the planet's Love number  $k_{2p}$  (Ragozzine & Wolf 2009; Vissapragada et al. 2022):

$$\frac{d\omega}{dN} = 15\pi k_{2p} \left( \frac{M_*}{M_p} \right) \left( \frac{R_p}{a} \right)^5. \quad (8)$$

For a precession rate of  $38^{+25}_{-14}$  yr $^{-1}$  to be caused by planetary tidal bulges, the value of  $k_{2p}$  is  $270^{+180}_{-100}$ . The Love number  $k_2$  is a measure of the mass distribution inside a planet. The value is required to be between 0 and 1.5, with a homogeneous body yielding the maximum (Kramm et al. 2011). This calculated value is much larger than the maximum, and so is unphysical.

If the star is evolved the stellar tidal bulge may be a larger contributor to precession. If we calculate the stellar Love number  $k_{2*}$  using:

$$\frac{d\omega}{dN} = 15\pi k_{2*} \left( \frac{M_p}{M_*} \right) \left( \frac{R_*}{a} \right)^5, \quad (9)$$

we find a value of  $1.6^{+1.0}_{-0.6} \times 10^5$ , which is even larger. A higher eccentricity orbit decreases the required precession rate, so we can check whether any physical solution for  $k_{2p}$  can exist as  $e$  approaches 1. Using Equation 8, we can find that the precession rate is  $k_{2p} \times 0.14^\circ$  yr $^{-1}$ . To create the largest TTVs, the cosine term of Equation 5 must have a large derivative. Here the small-angle approximation for the change in value of the cosine term is parabolic, equal to  $\frac{1}{2}(\omega(N))^2$ . Across half the TTV baseline, the most that the planet can precess is  $k_{2p} \times 0.28^\circ$ , or  $k_{2p} \times 0.005$  radians, implying the cosine term can change by at most  $(k_{2p})^2 \times 1.25 \times 10^{-5}$ . Using Equation 5, we find  $\Delta t = e \times (k_{2p})^2 \times 1.6 \times 10^{-5}$  days, or  $e \times (k_{2p})^2 \times 0.023$  minutes. To get  $\Delta t$  of  $\sim 4$  minutes,  $e \times (k_{2p})^2 \sim 170$ . As the Love number has an upper bound of 1.5, this is not possible for any eccentricity.

Yee et al. (2023) report a circularization timescale of  $\sim 0.2$  Gyr and a stellar age of  $\sim 9.5$  Gyr. Using Equation 5, an eccentricity of  $\sim 0.001$  will result in a TTV amplitude of  $\sim 4$  minutes, so the eccentricity must be at least this value to produce the observed TTVs, regardless of precession rate. A highly eccentric orbit should be circularized below this value over a time period of 1-2 billion years. Without a mechanism to increase it, the eccentricity will be too small for apsidal precession to account for the observed TTVs.

Precession can also be caused by stellar oblateness (Sterne 1939). For a circular, aligned orbit the precession can be calculated using:

$$\frac{d\omega}{dN} = \frac{3}{2} J_2 \left( \frac{R_*}{a} \right)^2, \quad (10)$$

where  $J_2$  is the gravitational potential due to oblateness (Li et al. 2020). This value is typically  $\sim 10^{-7}$ . Here we find an asymmetric distribution for  $J_2$  of  $\log_{10}(J_2) = -0.42^{+0.24}_{-0.19}$ , many orders of magnitude larger, suggesting that oblateness cannot cause the required precession.

### 3.5. A Near-Resonant Planet

Another possible cause of the TTVs is perturbations from a low-mass, nearby planet. Such a planet needs a sufficiently low mass to evade detection in the ESPRESSO data. A planet with a small radius and large TTVs may be difficult to detect in *TESS* data even if transiting. In order to test this possibility we simulate a planet with an orbital period near different inner and outer mean-motion resonances of TOI-2818 b. These configurations induce detectable TTVs even for a small planet, and cause the TTVs to have a longer super-period in their trends in order to cover the long *TESS* baseline.

The resulting fits are poorly constrained by the lack of information about the second planet. Without further transits or additional RV measurements, a unique solution cannot be obtained. We present multiple best fit solutions for different orbital periods to demonstrate the plausibility of a planet as the cause of the TTVs. In all tested periods, a planet in the  $\lesssim 10M_{\oplus}$  mass range is sufficient to reproduce the TTVs; these planets would not be seen in ESPRESSO data. An example given by the best-fitting 16-day planet model is listed in Table 3. This features the largest planet at  $\sim 10M_{\oplus}$ , while the similar TTV curve of the 12-day solution has a  $< 1M_{\oplus}$  planet. The 16-day solution decreases the mass of planet b by  $0.1M_{\text{Jup}}$ , while the other solutions do not significantly change the mass of the hot Jupiter. The best fitting TTV model for planets on 16-, 12-, 8- and 1-day orbits are shown in Figure 1.

We find that as the orbit of the outer planet becomes wider, the change in TTVs becomes slower. The 12- and 16-day orbits produce lower frequency TTVs that better match the *TESS* observing cadence.

We integrate each of the best-fitting solutions to test the stability of these configurations with REBOUND (Rein & Liu 2012; Rein & Spiegel 2015). We find that these systems are stable over a period of at least 100,000 years.

### 3.6. Constraints on Potential Moons

The existence of a moon can create TTVs by moving the planet around the barycenter of the planet-moon system. To maximize the size of the TTVs, we consider a moon at half the Hill radius (Domingos et al. 2006). In this system, half the Hill radius is  $\approx 220,000$  km. The orbital velocity of the planet is  $\approx 8100$  km  $\text{min}^{-1}$ . A moon of  $\approx 15M_{\oplus}$  at half the Hill radius is massive enough to shift the planet from the barycenter by 16,000 km, causing a TTV semi-amplitude of 2 minutes as observed. Such a small moon might not create an obvious transit signal on either side of the planet transit. For a sector of *TESS* transits to be early, the moon must be in the

same location for each transit. The orbital periods of the moon and planet must be very near an orbital commensurability, an unlikely but not impossible coincidence. Continued TTV monitoring could enable inference of a unique candidate moon solution which could be tested with high-precision photometric observations by *HST* or *JWST*.

## 4. CONCLUSIONS

TOI-2818 b shows TTVs that deviate from a constant period over a 4 year baseline of *TESS* data. Multiple models are able to fit the transit times, but are inconsistent with either the radial velocity measurements, or our knowledge of planet structure and tides. The preferred model we investigated that can explain the data invokes gravitational perturbations from a small nearby planet, although the data are insufficient to find a single solution. More observations in the form of additional transits and high precision radial velocity measurements are necessary to confirm and characterize the second planet. The old age of this system is significant as it shows that such a system can exist after billions of year, without the orbits decaying or becoming unstable. This is suggestive of smooth disk migration leading to the current orbital configuration. The rates of hot Jupiters with and without TTVs due to companion planets will reveal the relative rates of formation through smooth disk migration, which will preserve companions in orbital resonances, and high eccentricity migration, which will lead to the scattering of companions. This system, a hot Jupiter with a likely companion around an evolved star with a precisely known age, can provide a benchmark to better understand the lifetimes of hot Jupiters and their environments.

## ACKNOWLEDGMENTS

We thank João Faria for constructive discussions that improved the quality of this manuscript.

We thank the anonymous referee for their prompt and helpful feedback.

This research made use of `exoplanet` (Foreman-Mackey et al. 2021a,b) and its dependencies (Agol et al. 2020; Kumar et al. 2019; Astropy Collaboration et al. 2013, 2018; Luger et al. 2019; Salvatier et al. 2016; Theano Development Team 2016).

This paper includes data collected with the *TESS* mission, obtained from the MAST data archive at the Space Telescope Science Institute (STScI). The specific observations analyzed can be accessed via <https://doi.org/10.17909/0cp4-2j79> (STScI 2022) and <https://doi.org/10.17909/t9-nmc8-f686> (STScI 2021). Funding for the *TESS* mission is provided by the NASA

Explorer Program. STScI is operated by the Association of Universities for Research in Astronomy, Inc., under NASA contract NAS 5–26555.

This research has made use of the Exoplanet Follow-up Observation Program website, which is operated by the California Institute of Technology, under contract with the National Aeronautics and Space Administration under the Exoplanet Exploration Program.

This research has used data from the SMARTS 1.5m telescope, which is operated as part of the SMARTS Consortium. Based in part on observations at NSF Cerro Tololo Inter-American Observatory, NSF NOIR-Lab, which is managed by the Association of Universities for Research in Astronomy (AURA) under a cooperative agreement with the U.S. National Science Foundation.

Based on observations collected at the European Southern Observatory under ESO programme 111.264Q (PI Montet).

This work has made use of data from the European Space Agency (ESA) mission *Gaia* (<https://www.cosmos.esa.int/gaia>), processed by the *Gaia* Data Processing and Analysis Consortium (DPAC, <https://www.cosmos.esa.int/web/gaia/dpac/consortium>). Funding for the DPAC has been provided by national institutions, in particular the institutions participating in the *Gaia* Multilateral Agreement.

B.J.M. is supported by an Australian Government Research Training Program (RTP) Scholarship.

J.H.C.M. is supported by FCT - Fundação para a Ciência e a Tecnologia through national funds by these grants: UIDB/04434/2020, UIDP/04434/2020, PTDC/FIS-AST/4862/2020. J.H.C.M. is also supported by the European Union (ERC, FIERCE, 101052347).

A.M.S acknowledges support from the Fundação para a Ciência e a Tecnologia (FCT) through the Fellowship 2020.05387.BD (DOI: 10.54499/2020.05387.BD). Funded/Co-funded by the European Union (ERC, FIERCE, 101052347). Views and opinions expressed are however those of the author(s) only and do not necessarily reflect those of the European Union or the European Research Council. Neither the European Union nor the granting authority can be held responsible for them. This work was supported by FCT - Fundação para a Ciência e a Tecnologia through national funds by these grants: UIDB/04434/2020, UIDP/04434/2020.

*Facilities:* TESS, El Sauce: 0.6m, LCOGT, CTIO:1.5m (CHIRON), VLT:Antu (ESPRESSO)

*Software:* arviz (Kumar et al. 2019), Astropy (Astropy Collaboration et al. 2013, 2018), astroquery (Ginsburg et al. 2019), emcee (Foreman-Mackey et al. 2013), exoplanet (Foreman-Mackey et al. 2021a,b), Lightkurve (Lightkurve Collaboration et al. 2018), Matplotlib (Hunter 2007), NumPy (Harris et al. 2020), PyMC3 (Salvatier et al. 2016), REBOUND (Rein & Liu 2012; Rein & Spiegel 2015), SciPy (Virtanen et al. 2020), starry (Luger et al. 2019) Theano (Theano Development Team 2016), TTVFast (Deck et al. 2014),

## REFERENCES

- Agol, E., Luger, R., & Foreman-Mackey, D. 2020, *AJ*, 159, 123, doi: [10.3847/1538-3881/ab4fee](https://doi.org/10.3847/1538-3881/ab4fee)
- Astropy Collaboration, Robitaille, T. P., Tollerud, E. J., et al. 2013, *A&A*, 558, A33, doi: [10.1051/0004-6361/201322068](https://doi.org/10.1051/0004-6361/201322068)
- Astropy Collaboration, Price-Whelan, A. M., Sipőcz, B. M., et al. 2018, *AJ*, 156, 123, doi: [10.3847/1538-3881/aabc4f](https://doi.org/10.3847/1538-3881/aabc4f)
- Barker, A. J. 2020, *MNRAS*, 498, 2270, doi: [10.1093/mnras/staa2405](https://doi.org/10.1093/mnras/staa2405)
- Becker, J. C., Vanderburg, A., Adams, F. C., Rappaport, S. A., & Schwengeler, H. M. 2015, *ApJL*, 812, L18, doi: [10.1088/2041-8205/812/2/L18](https://doi.org/10.1088/2041-8205/812/2/L18)
- Belokurov, V., Penoyre, Z., Oh, S., et al. 2020, *MNRAS*, 496, 1922, doi: [10.1093/mnras/staa1522](https://doi.org/10.1093/mnras/staa1522)
- Borkovits, T., Hajdu, T., Sztakovics, J., et al. 2016, *MNRAS*, 455, 4136, doi: [10.1093/mnras/stv2530](https://doi.org/10.1093/mnras/stv2530)
- Bouma, L. G., Winn, J. N., Howard, A. W., et al. 2020, *ApJL*, 893, L29, doi: [10.3847/2041-8213/ab8563](https://doi.org/10.3847/2041-8213/ab8563)
- Cañas, C. I., Wang, S., Mahadevan, S., et al. 2019, *ApJL*, 870, L17, doi: [10.3847/2041-8213/aafa1e](https://doi.org/10.3847/2041-8213/aafa1e)
- Deck, K. M., Agol, E., Holman, M. J., & Nesvorný, D. 2014, *ApJ*, 787, 132, doi: [10.1088/0004-637x/787/2/132](https://doi.org/10.1088/0004-637x/787/2/132)
- Domingos, R. C., Winter, O. C., & Yokoyama, T. 2006, *MNRAS*, 373, 1227, doi: [10.1111/j.1365-2966.2006.11104.x](https://doi.org/10.1111/j.1365-2966.2006.11104.x)
- Foreman-Mackey, D., Hogg, D. W., Lang, D., & Goodman, J. 2013, *PASP*, 125, 306, doi: [10.1086/670067](https://doi.org/10.1086/670067)
- Foreman-Mackey, D., Luger, R., Agol, E., et al. 2021a, arXiv e-prints, arXiv:2105.01994, <https://arxiv.org/abs/2105.01994>
- Foreman-Mackey, D., Savel, A., Luger, R., et al. 2021b, exoplanet-dev/exoplanet v0.5.1, doi: [10.5281/zenodo.1998447](https://doi.org/10.5281/zenodo.1998447)
- Gaia Collaboration, Prusti, T., de Bruijne, J. H. J., et al. 2016, *A&A*, 595, A1, doi: [10.1051/0004-6361/201629272](https://doi.org/10.1051/0004-6361/201629272)

- Gaia Collaboration, Vallenari, A., Brown, A. G. A., et al. 2023, *A&A*, 674, A1, doi: [10.1051/0004-6361/202243940](https://doi.org/10.1051/0004-6361/202243940)
- Geweke, J. 1992, *Bayesian Statistics IV*. Oxford: Clarendon Press, ed. J. M. Bernardo, 169
- Giménez, A., & Bastero, M. 1995, *Ap&SS*, 226, 99, doi: [10.1007/BF00626903](https://doi.org/10.1007/BF00626903)
- Ginsburg, A., Sipőcz, B. M., Brasseur, C. E., et al. 2019, *AJ*, 157, 98, doi: [10.3847/1538-3881/aafc33](https://doi.org/10.3847/1538-3881/aafc33)
- Goldreich, P., & Soter, S. 1966, *Icarus*, 5, 375, doi: [10.1016/0019-1035\(66\)90051-0](https://doi.org/10.1016/0019-1035(66)90051-0)
- Goodman, J., & Weare, J. 2010, *Communications in Applied Mathematics and Computational Science*, 5, 65, doi: [10.2140/camcos.2010.5.65](https://doi.org/10.2140/camcos.2010.5.65)
- Harris, C. R., Millman, K. J., van der Walt, S. J., et al. 2020, *Nature*, 585, 357, doi: [10.1038/s41586-020-2649-2](https://doi.org/10.1038/s41586-020-2649-2)
- Hord, B. J., Colón, K. D., Kostov, V., et al. 2021, *The Astronomical Journal*, 162, 263, doi: [10.3847/1538-3881/ac2602](https://doi.org/10.3847/1538-3881/ac2602)
- Hord, B. J., Colón, K. D., Berger, T. A., et al. 2022, *The Astronomical Journal*, 164, 13, doi: [10.3847/1538-3881/ac6f57](https://doi.org/10.3847/1538-3881/ac6f57)
- Huang, C. X., Quinn, S. N., Vanderburg, A., et al. 2020, *The Astrophysical Journal*, 892, L7, doi: [10.3847/2041-8213/ab7302](https://doi.org/10.3847/2041-8213/ab7302)
- Huang, C. X., Vanderburg, A., Pál, A., et al. 2020a, *Research Notes of the American Astronomical Society*, 4, 204, doi: [10.3847/2515-5172/abca2e](https://doi.org/10.3847/2515-5172/abca2e)
- . 2020b, *Research Notes of the American Astronomical Society*, 4, 206, doi: [10.3847/2515-5172/abca2d](https://doi.org/10.3847/2515-5172/abca2d)
- Hunter, J. D. 2007, *Computing in Science and Engineering*, 9, 90, doi: [10.1109/MCSE.2007.55](https://doi.org/10.1109/MCSE.2007.55)
- Jang-Condell, H. 2015, *ApJ*, 799, 147, doi: [10.1088/0004-637X/799/2/147](https://doi.org/10.1088/0004-637X/799/2/147)
- Jenkins, J. M., Twicken, J. D., McCauliff, S., et al. 2016, in *Society of Photo-Optical Instrumentation Engineers (SPIE) Conference Series*, Vol. 9913, *Software and Cyberinfrastructure for Astronomy IV*, ed. G. Chiozzi & J. C. Guzman, 99133E, doi: [10.1117/12.2233418](https://doi.org/10.1117/12.2233418)
- Kipping, D. M. 2013, *MNRAS*, 435, 2152, doi: [10.1093/mnras/stt1435](https://doi.org/10.1093/mnras/stt1435)
- Korth, J., Gandolfi, D., Šubjak, J., et al. 2023, *A&A*, 675, A115, doi: [10.1051/0004-6361/202244617](https://doi.org/10.1051/0004-6361/202244617)
- Kramm, U., Nettelmann, N., Redmer, R., & Stevenson, D. J. 2011, *A&A*, 528, A18, doi: [10.1051/0004-6361/201015803](https://doi.org/10.1051/0004-6361/201015803)
- Kumar, R., Carroll, C., Hartikainen, A., & Martin, O. A. 2019, *The Journal of Open Source Software*, doi: [10.21105/joss.01143](https://doi.org/10.21105/joss.01143)
- Kunimoto, M., Huang, C., Tey, E., et al. 2021, *Research Notes of the American Astronomical Society*, 5, 234, doi: [10.3847/2515-5172/ac2ef0](https://doi.org/10.3847/2515-5172/ac2ef0)
- Li, G., Dai, F., & Becker, J. 2020, *ApJL*, 890, L31, doi: [10.3847/2041-8213/ab72f4](https://doi.org/10.3847/2041-8213/ab72f4)
- Lightkurve Collaboration, Cardoso, J. V. d. M., Hedges, C., et al. 2018, *Lightkurve: Kepler and TESS time series analysis in Python*, *Astrophysics Source Code Library*. <http://ascl.net/1812.013>
- Lindgren, L., Hernández, J., Bombrun, A., et al. 2018, *A&A*, 616, A2, doi: [10.1051/0004-6361/201832727](https://doi.org/10.1051/0004-6361/201832727)
- Lindgren, L., Klioner, S. A., Hernández, J., et al. 2021, *A&A*, 649, A2, doi: [10.1051/0004-6361/202039709](https://doi.org/10.1051/0004-6361/202039709)
- Luger, R., Agol, E., Foreman-Mackey, D., et al. 2019, *AJ*, 157, 64, doi: [10.3847/1538-3881/aae8e5](https://doi.org/10.3847/1538-3881/aae8e5)
- Maciejewski, G., Golonka, J., Loboda, W., et al. 2023, *MNRAS*, 525, L43, doi: [10.1093/mnras/lsad078](https://doi.org/10.1093/mnras/lsad078)
- McKee, B. J., & Montet, B. T. 2023, *AJ*, 165, 236, doi: [10.3847/1538-3881/accd66](https://doi.org/10.3847/1538-3881/accd66)
- NExSci. 2022, *Exoplanet Follow-up Observing Program Web Service, IPAC*, doi: [10.26134/EXOFOP5](https://doi.org/10.26134/EXOFOP5)
- Paredes, L. A., Henry, T. J., Quinn, S. N., et al. 2021, *AJ*, 162, 176, doi: [10.3847/1538-3881/ac082a](https://doi.org/10.3847/1538-3881/ac082a)
- Patra, K. C., Winn, J. N., Holman, M. J., et al. 2017, *The Astronomical Journal*, 154, 4, doi: [10.3847/1538-3881/aa6d75](https://doi.org/10.3847/1538-3881/aa6d75)
- . 2020, *The Astronomical Journal*, 159, 150, doi: [10.3847/1538-3881/ab7374](https://doi.org/10.3847/1538-3881/ab7374)
- Pepe, F., Cristiani, S., Rebolo, R., et al. 2021, *A&A*, 645, A96, doi: [10.1051/0004-6361/202038306](https://doi.org/10.1051/0004-6361/202038306)
- Ragozzine, D., & Wolf, A. S. 2009, *ApJ*, 698, 1778, doi: [10.1088/0004-637X/698/2/1778](https://doi.org/10.1088/0004-637X/698/2/1778)
- Rein, H., & Liu, S. F. 2012, *A&A*, 537, A128, doi: [10.1051/0004-6361/201118085](https://doi.org/10.1051/0004-6361/201118085)
- Rein, H., & Spiegel, D. S. 2015, *MNRAS*, 446, 1424, doi: [10.1093/mnras/stu2164](https://doi.org/10.1093/mnras/stu2164)
- Ricker, G. R., Winn, J. N., Vanderspek, R., et al. 2015, *Journal of Astronomical Telescopes, Instruments, and Systems*, 1, 014003, doi: [10.1117/1.JATIS.1.1.014003](https://doi.org/10.1117/1.JATIS.1.1.014003)
- Salvatier, J., Wiecki, T. V., & Fonnesbeck, C. 2016, *PeerJ Computer Science*, 2, e55
- Sha, L., Vanderburg, A. M., Huang, C. X., et al. 2023, *MNRAS*, 524, 1113, doi: [10.1093/mnras/stad1666](https://doi.org/10.1093/mnras/stad1666)
- Smith, J. C., Stumpe, M. C., Cleve, J. E. V., et al. 2012, *PASP*, 124, 1000, doi: [10.1086/667697](https://doi.org/10.1086/667697)
- Sterne, T. E. 1939, *MNRAS*, 99, 451, doi: [10.1093/mnras/99.5.451](https://doi.org/10.1093/mnras/99.5.451)
- STScI. 2021, *TESS Light Curves - All Sectors*, STScI/MAST, doi: [10.17909/T9-NMC8-F686](https://doi.org/10.17909/T9-NMC8-F686)

- STScI. 2022, TESS Calibrated Full Frame Images: All Sectors, STScI/MAST, doi: [10.17909/0CP4-2J79](https://doi.org/10.17909/0CP4-2J79)
- Stumpe, M. C., Smith, J. C., Catanzarite, J. H., et al. 2014, PASP, 126, 100, doi: [10.1086/674989](https://doi.org/10.1086/674989)
- Theano Development Team. 2016, arXiv e-prints, abs/1605.02688. <http://arxiv.org/abs/1605.02688>
- Tokovinin, A., Fischer, D. A., Bonati, M., et al. 2013, PASP, 125, 1336, doi: [10.1086/674012](https://doi.org/10.1086/674012)
- Virtanen, P., Gommers, R., Oliphant, T. E., et al. 2020, Nature Methods, 17, 261, doi: [10.1038/s41592-019-0686-2](https://doi.org/10.1038/s41592-019-0686-2)
- Vissapragada, S., Chontos, A., Greklek-McKeon, M., et al. 2022, The Astrophysical Journal Letters, 941, L31, doi: [10.3847/2041-8213/aca47e](https://doi.org/10.3847/2041-8213/aca47e)
- Wallace, A. L., Casey, A. R., Brown, A. G. A., & Castro-Ginard, A. 2024, arXiv e-prints, arXiv:2411.06705, doi: [10.48550/arXiv.2411.06705](https://doi.org/10.48550/arXiv.2411.06705)
- Weinberg, N. N., Sun, M., Arras, P., & Essick, R. 2017, The Astrophysical Journal, 849, L11, doi: [10.3847/2041-8213/aa9113](https://doi.org/10.3847/2041-8213/aa9113)
- Wu, D.-H., Rice, M., & Wang, S. 2023, AJ, 165, 171, doi: [10.3847/1538-3881/acbf3f](https://doi.org/10.3847/1538-3881/acbf3f)
- Yee, S. W., Winn, J. N., Knutson, H. A., et al. 2020, ApJL, 888, L5, doi: [10.3847/2041-8213/ab5c16](https://doi.org/10.3847/2041-8213/ab5c16)
- Yee, S. W., Winn, J. N., Hartman, J. D., et al. 2023, ApJS, 265, 1, doi: [10.3847/1538-4365/aca286](https://doi.org/10.3847/1538-4365/aca286)